Available online at www.sciencedirect.com

SciVerse ScienceDirect

Journal of the European Ceramic Society 32 (2012) 2405–2414

www.elsevier.com/locate/jeurceramsoc

Development of multilayer textured $Ca_3Co_4O_9$ materials for thermoelectric generators: Influence of the anisotropy on the transport properties

Driss Kenfaui [a,*], Bertrand Lenoir [b], Daniel Chateigner [a], Bachir Ouladdiaf [c], Moussa Gomina [a], Jacques Guillaume Noudem [a]

[a] *CRISMAT, UMR 6508 CNRS/ENSICAEN, LUSAC, IUT-Caen and Université de Caen Basse-Normandie, 6 Bd Maréchal Juin, 14050 Caen Cedex 04, France*
[b] *Institut Jean Lamour, UMR 7198 CNRS-Nancy Université-UPVM, Ecole Nationale Supérieure des Mines de Nancy, Parc de Saurupt, 54042 Nancy, France*
[c] *Institut Laue-Langevin (ILL), 6 rue J. Horowitz, BP 156-38042 Grenoble Cedex 09, France*

Received 13 January 2012; received in revised form 11 March 2012; accepted 15 March 2012
Available online 7 April 2012

Abstract

Multilayer $Ca_3Co_4O_9$ (349) thick thermoelectric (TE) materials were fabricated by hot-pressing stacked dense and strongly textured single-layer samples. Microstructure and volume quantitative texture investigations were undertaken by using scanning electron microscopy and neutron diffraction techniques, respectively. The results show a bulk density similar to single-layer samples, but remarkable texture strength reinforcement. The electrical resistivity, ρ, and Seebeck coefficient, S, were reproducibly measured in directions parallel (ρ^c and S^c) and perpendicular (ρ^{ab} and S^{ab}) to the mean c-axis. ρ showed a high anisotropy ratio ρ^c/ρ^{ab} of 13.5 and 8.8 at 300 and 900 K, respectively, and ρ^{ab} kept the same values whereas ρ^c decreased in the multilayer samples. S^{ab} and S^c unexpectedly revealed different values. The thermal conductivity also displayed a significant anisotropy, with ratio $\kappa^{ab}/\kappa^c = 2.7$ at 900 K. The resulting figure-of-merit ZT is then noticeably anisotropic, with ratio $ZT^{ab}/ZT^c = 4.6$. ZT^{ab} was found 2 times larger than ZT value of the conventional sintered 349 materials often used for TE modules fabrication.

Keywords: $Ca_3Co_4O_9$ oxides; Hot pressing; Electrical properties; Thermal conductivity; Functional applications

1. Introduction

Degenerate semiconducting materials have been used for thermoelectric (TE) applications for more than 60 years, whereas TE oxides have been considered as not appropriate owing to their high thermal conductivity. Nonetheless, layered cobaltite oxides have been reported to exhibit unexpected TE properties in the last fifteen years,[1–3] which has noticeably stimulated the experimental studies on this family of materials with the aim to attain a sufficient TE conversion efficiency for extensive applicative uses. Indeed, after the discovery of a large thermopower (Seebeck coefficient) in $NaCo_2O_4$[1] and $Ca_3Co_4O_9$[2] oxides, various studies were reported,[4] showing high Seebeck coefficient, S^{ab}, concomitant with low resistivity, ρ^{ab}, and low thermal conductivity, κ^{ab}, in the in-plane (i.e. (a, b) planes) of $Ca_3Co_4O_9$ materials. It results then a good (a, b) planes TE conversion efficiency defined by the figure-of-merit $ZT^{ab} = (S^{ab^2} \times T)/(\rho^{ab} \times \kappa^{ab})$ of 0.3–0.4 at 950–1100 K, where T refers to the absolute temperature. Besides its TE performance, $Ca_3Co_4O_9$ oxide is also characterized by a high oxidation resistance, excellent chemical and thermal stabilities in air at high temperature and no toxic character of its elements, natural merits which make this material one of the most serious candidates for future TE applications in the high temperature range. The $Ca_3Co_4O_9$ crystal structure consists of CdI_2-type hexagonal CoO_2 layers and NaCl-type Ca_2CoO_3 layers alternatively stacked along the c-axis[2]; the $Ca_3Co_4O_9$ phase is thus a composite crystal with b-axis lattice misfit. Such layered structure induces a strong TE properties anisotropy. This anisotropy has been already evidenced for the resistivity[2,5–8] but never for the Seebeck coefficient, which is still considered as an isotropic property in the literature regardless of the crystal structure, though its anisotropic character has been described formerly by using asymmetric 3×3 tensors.[9]

* Corresponding author. Tel.: +33 231 45 13 20; fax: +33 231 45 13 09.
E-mail address: driss.kenfaui@grenoble.cnrs.fr (D. Kenfaui).

0955-2219/$ – see front matter © 2012 Elsevier Ltd. All rights reserved.
doi:10.1016/j.jeurceramsoc.2012.03.022

On the other hand, a large-size $Ca_3Co_4O_9$ single crystal is very difficult to grow, and a bulk single crystal shaped to be applied directly as TE devices practically impossible to elaborate. However, polycrystalline bulks exhibit low *ZT* values, especially when processed by using the conventional sintering – CS. Several processes (hot pressing – HP, spark plasma sintering – SPS, reactive template growth – RTG, etc.)[6–8,10] have been then explored to consolidate the $Ca_3Co_4O_9$ ceramics in view of minimizing current flow barriers and thereby reducing mean (*a*, *b*) planes electrical resistivity, ρ^{ab}.

We have recently highlighted[7] that HP is very effective for processing dense and strongly textured $Ca_3Co_4O_9$ single-layer samples with a significant (*a*, *b*) planes grain growth, which reduces significantly their electrical resistivity, ρ^{ab}, and consequently, improves their power factor, $PF^{ab} = S^{ab^2}/\rho^{ab}$. Nevertheless, the obtained single-layer samples are still too thin (with a mean thickness of about 0.5 mm) to design TE ceramic elements 'legs' with dimensions (length and section of at least ~5 mm and ~4 mm × 4 mm, respectively) as required for high temperature TE modules fabrication.[11–13]

To overcome this problem, we have fabricated a thick $Ca_3Co_4O_9$ sample (multilayer) by stacking and hot-pressing strongly textured $Ca_3Co_4O_9$ single-layer samples along their mean *c*-axis by using HP process. Microstructure and texture were investigated in the core of the processed materials. Electrical resistivity, Seebeck coefficient and thermal conductivity were together measured, for the first time to our knowledge, in both directions: parallel and perpendicular to the mean *c*-axis of the multilayer sample. A rigorous study of the TE properties anisotropy has been then undertaken.

2. Experimental procedure

2.1. Processing

The details of the preparation process of dense $Ca_3Co_4O_9$ bulk textured materials by using hot-pressing (HP) have been recently reported.[7] Briefly, the powder was synthesized from the starting precursors $CaCO_3$ and Co_3O_4 by using the solid-state reaction method. The raw powder was initially mixed in an agate ball mill and then calcined in air at 900 °C for 24 h. The obtained powder was finely ground, and then uniaxially cold-pressed at 95 MPa into pellets 4 mm thick and 25 mm in diameter. The pellet was then set in the furnace[14] between two 0.125 mm-thick silver sheets to avoid any reaction with alumina-bearing plates during heating. The employed uniaxial stress was fixed at 30 MPa and the dwell temperature at 920 °C for 24 h.[7] The resulting $Ca_3Co_4O_9$ discs had a mean thickness of about 0.5 mm, and exhibited microstructure features of a dense and strongly textured bulk sample, with the highest texture strength[7] ever seen in such bulk materials.

Thirty $Ca_3Co_4O_9$ pellets were then textured by using HP process under the conditions mentioned above, and cut into ~18 mm × 18 mm × 0.5 mm parallelepiped single-layer samples. Before the stacking stage, the single-layer samples were mirror-polished on their two faces using polishing paper down to 1 μm, and their final thickness was decreased to 0.3–0.4 mm. They were thereafter stacked along their mean *c*-axis, without using any soldering agent, and hot-pressed at 920 °C and under a moderate uniaxial pressure of 10 MPa for 10 h (Fig. 1a). The thickness of the resulting thick sample is about 9 mm (Fig. 1b); the total time spent into the HP device for this elaboration is 1102 h.

Taking into account that this preparation is time-consuming and requires an important quantity of $Ca_3Co_4O_9$ powder, we prepared thinner multilayer sample by hot-pressing a stack of only 5 single-layer samples in view to determine the optimized experimental conditions and to apprehend their influence on the microstructure and texture, before having undertaken the thick multilayer sample from 30 single-layer samples.

One of the cold-pressed pellets prepared at 920 °C for 24 h by using the conventional sintering (i.e. without any applied pressure) is the reference sample.

2.2. Microstructure and texture analysis

The microstructure of the prepared $Ca_3Co_4O_9$ ceramics was examined by means of a Carl Zeiss (Supra 55, Oberkochen, Germany) Scanning Electron Microscope (SEM). Volume quantitative texture investigations were performed on

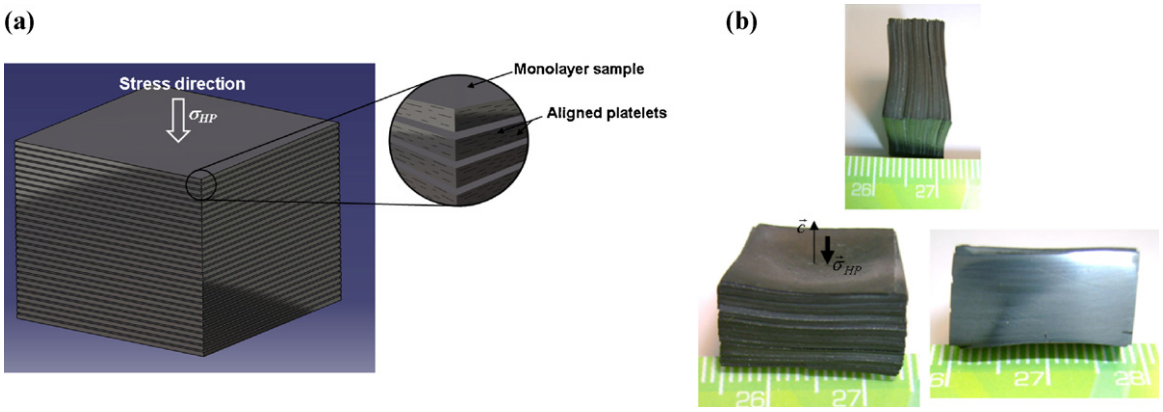

Fig. 1. (a) Hot-pressing stacking process used for fabricating the multilayer sample from 30 dense and strongly textured $Ca_3Co_4O_9$ single-layer samples. (b) The obtained multilayer sample and a view of its polished cross-section.

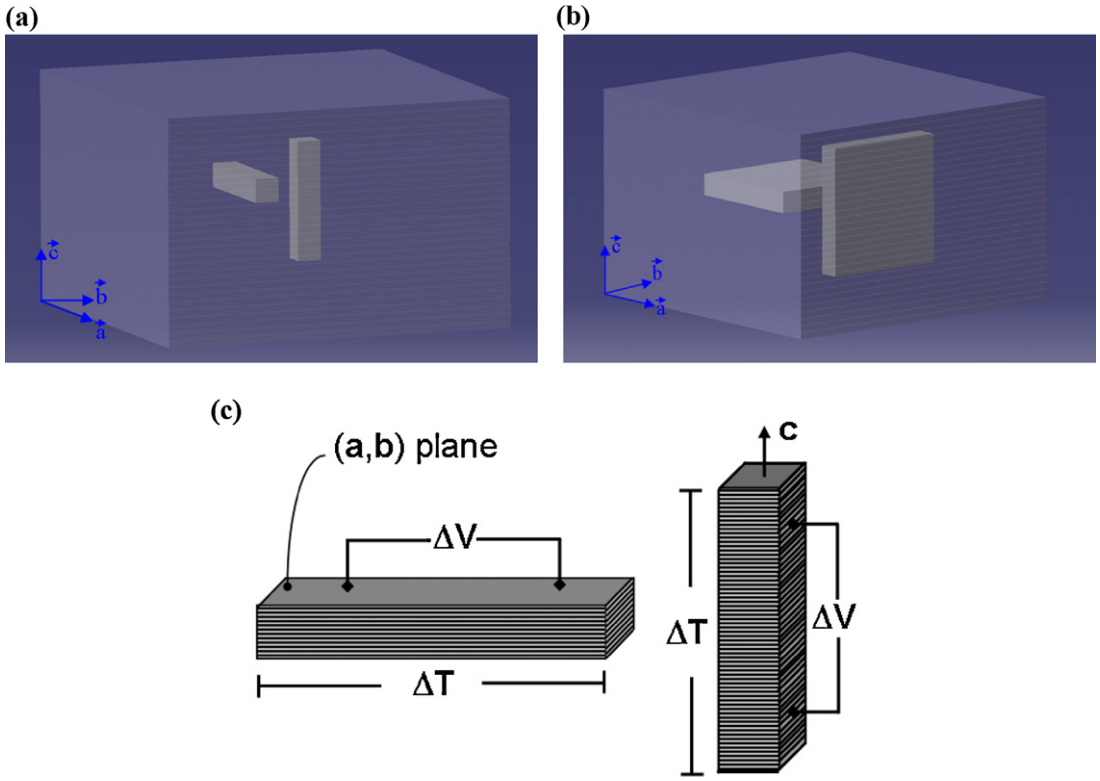

Fig. 2. Schematics of (a) bars and (b) parallelepiped specimens cut in the directions parallel and perpendicular to the applied pressing axis from the multilayer sample. (c) Schematic of the Seebeck coefficient, S, and the electrical resistivity, ρ, measurements in these two directions.

a ~8 mm × 6 mm × 7 mm parallelepiped specimen, cut from the core of the multilayer sample, using neutron diffraction. The newly developed 2D curved area position sensitive detector (CAPS) of the D19 beam line of the steady-state reactor of the Institut Laue-Langevin (ILL, Grenoble, France)[15] was used, and the sample mounted in the Eulerian cradle to provide the usual tilt (χ) and azimuth (φ) angle rotations. Because the CAPS detector spans 30° at once out of the diffractometer scattering plane, only 4 χ and 72 φ orientations of the sample in the cradle were necessary to cover the entire Orientation Distribution space. The whole diffraction pattern analysis was used in the combined Rietveld-EWIMV formalism,[15–17] implemented in the MAUD software.[18]

2.3. Thermoelectric characterizations

The temperature dependence of the electrical resistivity, ρ, and Seebeck coefficient, S, was measured parallel (ρ^c, S^c) and perpendicular (ρ^{ab}, S^{ab}) to the applied pressing axis. This latter is in fact aligned along the mean reciprocal c^* axis of the sample (we use the unique c-axis setting for the definition of the structure), but for the sake of simplicity, the reciprocal '*' symbol is avoided here.

In the temperature range from 5 to 350 K, $\rho^{ab}(T)$ and $\rho^c(T)$ were measured by the standard DC four-probe method by using a Quantum Design Physical Property Measurement System (PPMS, Oxford, Inc, UK). These measurements were performed on ~2 mm × 2 mm × 8 mm bar-shaped specimens for the 30-layers sample (Fig. 2a), and on ~4 mm × 4 mm × e (e is the thickness) parallelepiped-shaped samples for the single-layer and 5-layers samples,[7] cut by using a diamond saw (Struers, Champigny sur Marne, France). For the latter two samples, $\rho^c(T)$ was studied by using the Montgomery method.[19]

The contacts between the specimens and current leads were performed by painting commercially available silver paste (Dupont 4929) followed by an annealing in air at 900 °C for 2 h.

The high temperature (from 350 to 900 K) measurements of electrical resistivities, $\rho^{ab}(T)$ and $\rho^c(T)$, and Seebeck coefficients, $S^{ab}(T)$ and $S^c(T)$, were simultaneously monitored by means of a ZEM-3 apparatus (ULVAC-RIKO, Inc, Japan) and the four points contact method.

The thermal conductivity κ was determined in the 350–1000 K temperature range as follows: $\kappa = d \times C_p \times D$, where d and C_p are the density and the specific heat capacity, respectively, while D is the thermal diffusivity. C_p and d were measured by using the thermal analyzer (STA 449 F3 Jupiter®, NETZSCH-Gerätebau GmbH, Selb/Germany) and Archimedes method (KERN & Sohn GmbH, Baligen, Germany), respectively. D was measured by the laser flash diffusivity method by using the LFA 457 MicroFlash™ system (NETZSCH-Gerätebau GmbH, Selb/Germany) on ~6 mm × 6 mm × 2 mm parallelepiped-shaped specimens cut from the core of the 30-layers sample, in the directions parallel (D^c) and perpendicular (D^{ab}) to the applied pressing axis (Fig. 2b). Consequently, the thermal conductivity was determined, for the first time to our

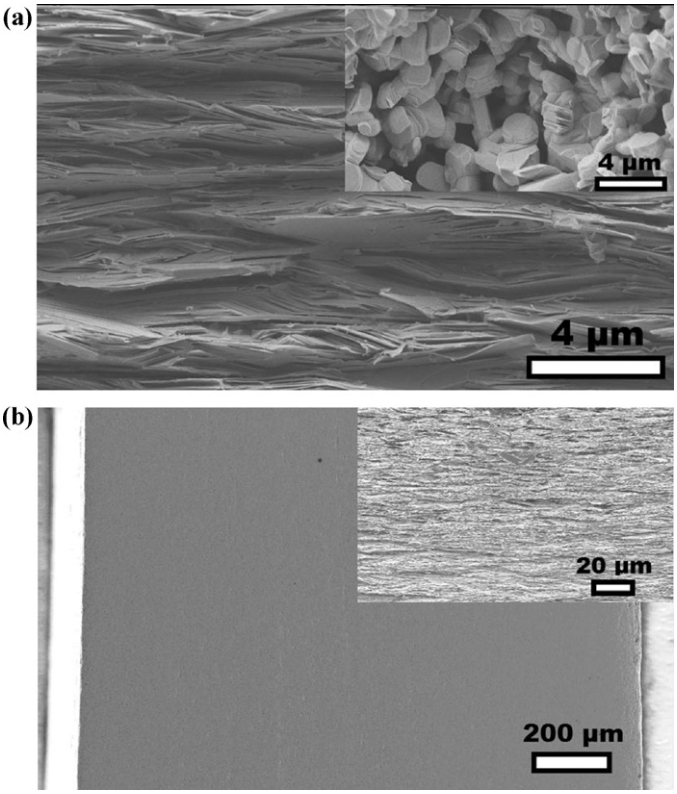

Fig. 3. (a) SEM micrographs of fractured surfaces of the $Ca_3Co_4O_9$ single-layer sample textured by the hot-pressing process under 30 MPa and at 920 for 24 h, and (inset) sample prepared by the conventional sintering. (b) Mirror-polished cross-sectional view of bar-shaped specimen cut perpendicular to the pressing axis from the core of the thick multilayer sample. Inset shows the internal alignment of the platelets in the initial discs of the multilayer sample.

knowledge, in the mean (a, b) planes (κ^{ab}) and in the planes containing the mean c*-axis (κ^{c}) of the textured $Ca_3Co_4O_9$ bulk materials.

3. Results and discussion

3.1. Microstructure

Fig. 3a shows a SEM micrograph of a fractured surface containing the pressing axis, illustrating a dense (96% of the theoretical density[2]) and homogeneous structure of the single-layer hot-pressed sample. It visibly reveals a high orientation degree of large grown platelets compactly stacked up along the pressing axis, in contrast with the reference sample processed without any applied pressure (inset of Fig. 3a). In fact, this latter sample is much porous (60% of the theoretical density) and presents smaller grains which appear to be randomly distributed and loosely assembled.

Fig. 3b illustrates the polished cross-sectional view of bar-shaped specimen cut parallel to the pressing axis from the core of the 30-layers sample. We could not distinguish any interface between the initial layers in the multilayer sample at this scale, which would favor the microstructural and physical properties homogeneity throughout the whole stack thickness. The hot-pressing stacking process promotes then the soldering of the primary layers to each other. From the inset of Fig. 3b, it appears that the internal alignment of the platelets in the initial discs of the multilayer sample was not perturbed by the hot-pressing stacking process. This was expected because the processing conditions are more moderated than those used for the single-layer samples consolidation. Indeed, one observes that the morphology of the multilayer sample exhibits a dense material with platelets strongly aligned along the whole stack thickness. Compared to the single-layer sample, the multilayer keeps almost the same relative bulk density (95%).

3.2. Texture studies

Fig. 4a exhibits a comparison between the two-dimensional experimental diagram obtained from the combined analysis of neutron diffraction on the parallelepiped-shaped specimen cut from the core of the thick multilayer sample, and the recalculated (refined) one by Rietveld refinement into the MAUD software. One observes a good reproducibility between measurements and refinement, with reliability factors ($R_w = 28.97\%$, $R_{Bragg} = 21.56\%$ and $R_{exp} = 32.26\%$) larger than those reported for $Ca_3Co_4O_9$ single-layer samples.[7] This is mainly related to the fact that the factors values depend also on the high number of the measurement points in this case. We recorded a goodness of fit (GoF) of only 1.8, which is an indication of a good global refinement.

On the other hand, the resulting refined cell parameters for the thick multilayer sample are $a = 4.8510(4)$ Å, $b = 36.361(4)$ Å and $c = 10.8572(5)$ Å, corresponding to (a, b) planes' (in-planes) contraction and out-of-planes' extension of about 0.0063, 0.165 Å and 0.0025 Å, respectively, compared to the single-layer sample. These cell modifications of the $Ca_3Co_4O_9$ structure probably occurred under the effect of the thermomechanical cycle applied during the hot-pressing stacking treatment, and are not analyzed further here.

The $\{0\,2\,0\}$, $\{0\,0\,1\}$ and $\{1\,0\,0\}$ pole figures, reconstructed after the combined refinement of the orientation distribution function (ODF), are given in Fig. 4b. This refinement is obtained with reliability factors $R_w = 27.53\%$ and $R_{Bragg} = 22.87\%$, coherent with the large value of the texture strength defined by the texture index,[20] $F^2 = 27.72$ mrd^2. These values are also much larger than those obtained for the single-layer sample ($R_w = 1.29\%$, $R_{Bragg} = 2.67\%$ and $F^2 = 6$ mrd^2).[7]

The obtained pole figures point clearly out that both the $\langle 0\,0\,1\rangle$* directions are strongly aligned parallel to the pressing axis and the platelets alignment was remarkably promoted under the hot-stacking pressing process. Indeed, the maximum of the $\{0\,0\,1\}$ poles is around 43 mrd, indicative of a texture strikingly two times stronger than the largest one we recently reported[7] for single-layer samples (22 mrd).

The maximum value of the orientation distribution (OD) is 121.6 mrd and its minimum is 0, which means that all the crystallites are oriented within the unique orientation component, i.e. the $\langle 0\,0\,1\rangle$* fiber texture with $\langle 0\,0\,1\rangle$*[15] directions are aligned parallel to the pressing axis of the thick multilayer sample. The inverse pole figure (Fig. 4c) determined for the pressing axis (ND) shows that indeed no other significant

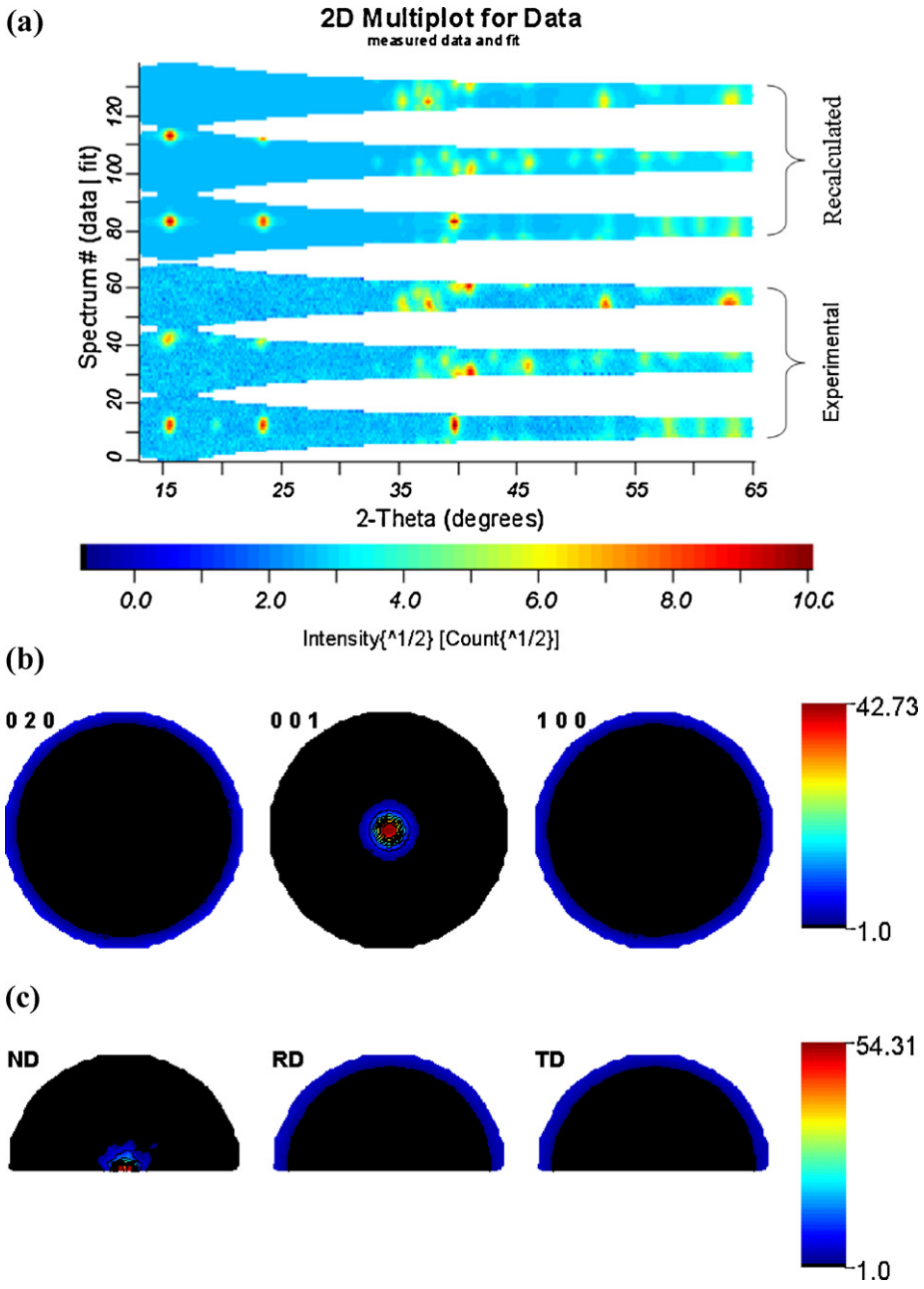

Fig. 4. (a) Two-dimensional experimental (bottom) and recalculated (top) diagrams measured after Rietveld refinement, (b) {0 2 0}, {0 0 1} and {1 0 0} recalculated normalized pole figures for the multilayer sample obtained after ODF refinement (linear density scale, equal area projection), and (c) inverse pole figure calculated for the direction of the pressure (logarithmic density scale, equal area projection).

orientation component than the ⟨0 0 1⟩* fiber exists and corresponds to levels of orientations along the pressure axis up to 54 mrd.

3.3. Anisotropic thermoelectrical properties

3.3.1. Electrical resistivity

Fig. 5a shows the temperature dependence of the electrical resistivity measured, in the 50–350 K range, parallel, ρ^c, and perpendicular, ρ^{ab}, to the mean c*-axis of the single-layer and the multilayer samples obtained by hot-pressing stacking of 5 and 30 layers. The curves show that the resistivity ρ^{ab} behavior neither depends on the number of stacked layers nor on the applied thermo-mechanical cycle. ρ^{ab} values for the 30-layers stack are similar to those obtained for the 5-layers one and for the single-layer sample. We can also observe that the resistivity ρ^{ab} was not influenced by the texture strength reinforcement noted for the 30-layers stack.

On the other hand, ρ^c decreases notably in the multilayer samples, as a consequence of the thermomechanical cycle which probably improves the connexion between platelets in the direction parallel to the mean c*-axis. However, the increase of the stacked layers number seems to oppose current circulation as we can see from the comparison between the 5-layers stack and

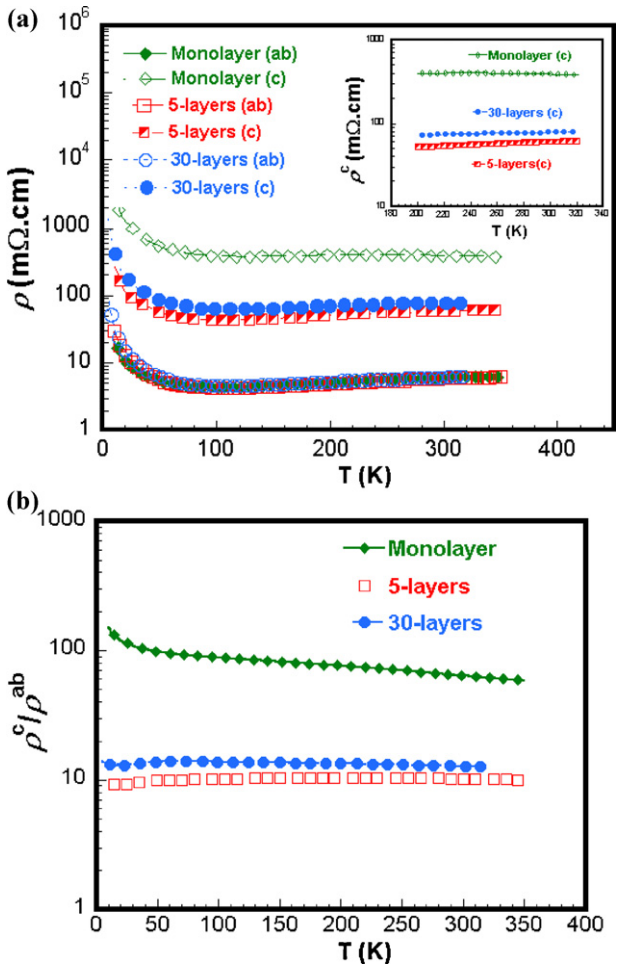

Fig. 5. (a) Temperature dependence of the electrical resistivity measured, in the 50-350 K range, in the mean (a, b) planes, ρ^{ab}, and parallel to the mean c-axis, ρ^{c}, of the single-layer sample and the multilayer samples obtained from the hot-pressing stacks of 5 and 30 layers. (b) Resulting temperature dependence of the resistivity anisotropy ratio, ρ^{c}/ρ^{ab}.

the 30-layers one (inset of Fig. 5a). Indeed, the latter displays ρ^{c} larger than that of the former because of the higher number of barriers imposed through interfaces by an increasing number stacked layer. ρ^{c} is 77.6 mΩ cm at 300 K for the 30-layers stack, corresponding to a reduction of about 5 times compared to the single-layer sample.

Owing to the ρ^{c} reduction in the thick samples, the anisotropy ratio ρ^{c}/ρ^{ab} is much lower than in the single-layer sample and appears roughly constant (Fig. 5b) in the probed temperature range. ρ^{c}/ρ^{ab} is slightly larger for the 30-layers stack compared with the 5-layers one. $\rho^{c}/\rho^{ab} = 13.5$ at 300 K for the thickest sample, close to single crystal values,[2,5] but at least 4 times larger than those published for textured $Ca_3Co_4O_9$ ceramics.[6,21]

Fig. 6a shows the dependence of the resistivity measured in the 300–900 K range parallel, ρ^{c}, and perpendicular, ρ^{ab}, to the mean c*-axis of the 30-layers sample. For each direction, these measurements were carried out on 4 different bars in view to check their reproducibility. The corresponding $\rho^{ab}(T)$ curve recorded for the single-layer is also plotted. One observes a good reproducibility of $\rho^{ab}(T)$ and $\rho^{c}(T)$ measured for the

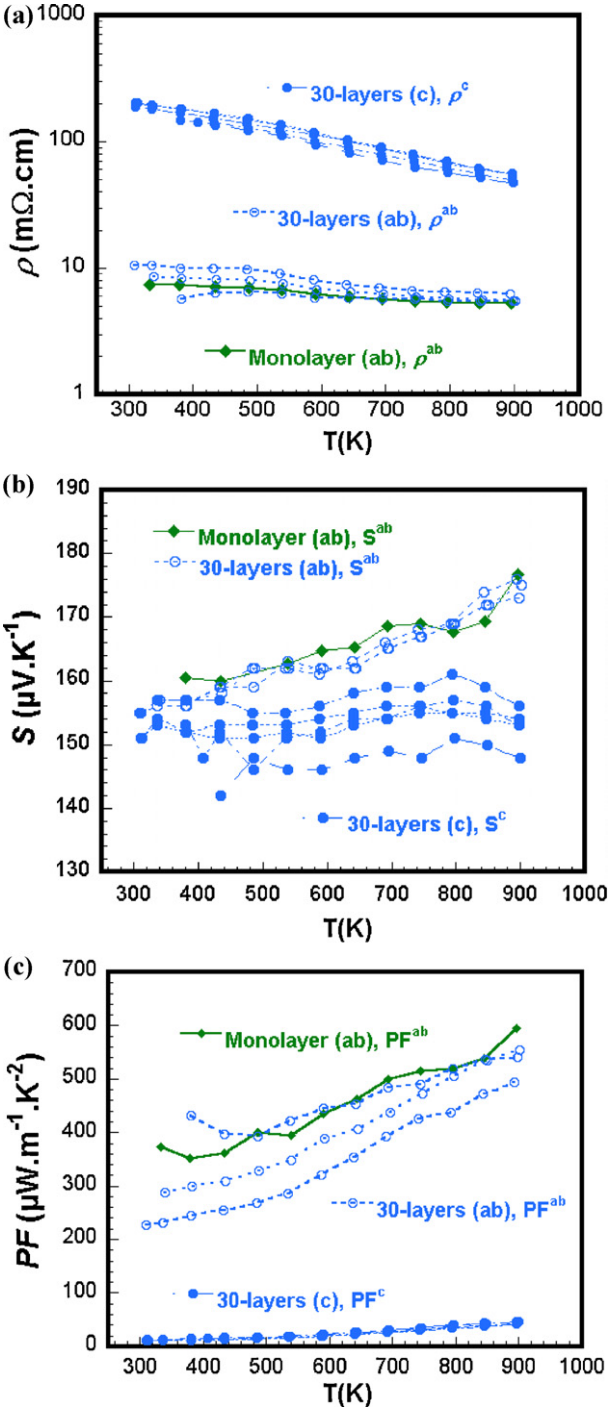

Fig. 6. Temperature dependence of (a) the electrical resistivity, (b) the Seebeck coefficient and (c) the resulting power factor, in the 350-900 K range, in the mean (a, b) planes (ρ^{ab}, S^{ab} and PF^{ab}) and parallel to the mean c*-axis (ρ^{c}, S^{c} and PF^{c}) of the multilayer samples obtained from the hot-pressing stacks of 5 and 30 layers. For the single-layer sample, only ρ^{ab}, S^{ab} and PF^{ab} are plotted.

multilayer sample, and the resistivity exhibits a spectacular anisotropy evidencing a big gap between ρ^{ab} and ρ^{c} values. Such a difference probably originates from:

(i) The strongly achieved texture which promotes electrical current flow in the mean (a, b) planes. However, even for a current injected parallel to the c*-axis (Fig. 2a), a part of it

flows in these planes for two mean reasons. On one hand, a number of the (a, b) planes are not exactly perpendicular to the axis of electrical current injection, which makes them contributing partly to the global conductivity in the (a, b) planes. On the other hand, we cannot, at the present time, exclude the ρ^{ac} (i.e. ρ^{13}) tensor component[22] which is not a priori equal to zero in such a monoclinic system. In principle, the texture effect on the electrical resistivity tends to achieve an anisotropy in resistivity at maximum the one of the single crystal. Furthermore, because of the fiber character of the achieved texture, the mean ρ^{ab} is also the mean value between ρ^{a} and ρ^{b}, which should be nonequal in this monoclinic crystal system. However, we are not aware of their independent determination on single crystals of $Ca_3Co_4O_9$, which would point for resistivity decrease using (a, b) planes alignment.

(ii) Within a single-layer, the grain boundary density is much larger in the mean planes parallel to the c*-axis than in the mean (a, b) planes, which results from the platelets' thickness $\leq$0.12 μm compared with their length $\leq$17 μm.[7] It induces a decrease in ρ^{ab}, but provokes a large elevation in ρ^{c}.

(iii) A high number of interfaces between primary single-layers of the stack sample opposing current flow in the mean c*-axis direction (Fig. 2a), which provokes another increase of ρ^{c}.

The average value of the anisotropy ratio, ρ^{c}/ρ^{ab}, is around 8.8 at 900 K, which is about 3 times larger than that reported by Zhang et al.,[6] but comparable to that obtained by Tani et al.[8] The resistivity ρ^{ab} of the single-layer sample exhibits the same values as those of the multilayer one, indicating that the texture reinforcement revealed after the hot-pressing stacking had not induced a noticeable effect on the current flow in the mean (a, b) planes. Considering a fiber texture type, one can see here a limit in its beneficial effect with respect to thermoelectric properties, if intrinsic anisotropy of crystallites is the sole concern. However extrinsic effects on resistivity, coming for instance from grain boundaries, can still be present and point for larger texture requirements.

3.3.2. Seebeck coefficient

Fig. 6b shows the Seebeck coefficient measured in the 300–900 K range on 4 bars cut parallel, S^{c}, and perpendicular, S^{ab}, to the mean c*-axis of the 30-layers sample. The $S^{ab}(T)$ curve of the single-layer sample is also plotted. As expected, this sample exhibits values similar to those of the 30-layers one (Fig. 6b), which, however, visibly presents S^{c} values different from those of S^{ab}. While Seebeck and Peltier coefficients are clearly represented by 2nd rank tensors,[9,22] they have never been measured as such to our knowledge, i.e. their anisotropic character has never been revealed experimentally, particularly on strongly textured polycrystalline materials. For a monoclinic crystal system, the Seebeck coefficient tensor of a single crystal is represented by $\begin{vmatrix} S_{11} & & S_{13} \\ & S_{22} & \\ S_{31} & & S_{33} \end{vmatrix}$, with 5 independent components. In our case of a textured polycrystalline materials exhibiting a $\langle 0\,0\,1\rangle$* fiber texture, the macroscopic symmetry imposes $S^{M}{}_{11} = S^{M}{}_{22}$ and $S^{M}{}_{13} = S^{M}{}_{31}$, i.e. only three independent components. We measured two Seebeck components, $S^{M}{}_{33} = S^{c}$, and $S^{M}{}_{11} = S^{ab}$, and $S^{M}{}_{13}$ is not determined. The observed anisotropy is reproducible and the $\Delta S = S^{ab} - S^{c}$ difference tends to increase as the temperature is raised, as we can see from Fig. 6b. There is only one similar result reported by Tani et al.[8] on textured $Ca_3Co_4O_9$ ceramics, but it was not commented in their paper. Furthermore, Yu et al.[23] have recently published a thermopower anisotropy for $La_{0.9}Ca_{0.1}MnO_3$ thin films, and such phenomena have been already observed in Sr_xCoO_2,[24] Ca_xCoO_2[25] and $YBa_2Cu_3O_{7-\delta}$[26,27] These results are in coherence with the tensorial expression of the Seebeck coefficient and support a thermopower effect more pronounced in the (a, b) planes than in the ones containing the c*-axis, as revealed for our strongly textured $Ca_3Co_4O_9$ polycrystalline materials. For a textured polycrystalline materials, the $S^{M}{}_{ij}$ values lie between the ones ($S^{M}{}_{ij}$) of the single crystal and the isotropic ones of a perfectly randomly oriented polycrystalline materials. Our samples are strongly textured with a narrow c*-axis distribution around the pellet axis (the FWHM of the distribution is not larger than 5°) and $S^{M}{}_{33}$ is probably close to the corresponding value of the single crystal. However, in the planes perpendicular to c*-axis, perfect isotropy is imposed by the fiber character of the texture[10] and $S^{M}{}_{11}$ is close to an averaged value between S_{11} and S_{22}.

Fig. 6c shows the temperature dependence of the power factor ($PF = S^2/\rho$) in the directions parallel, PF^{c}, and perpendicular, PF^{ab}, to the mean c*-axis of the 30-layers sample. To ease a comparison with the single-layer sample, the $PF^{ab}(T)$ curve of this latter is also plotted. One observes that PF^{ab} values of the multilayer sample present a higher dispersion than that of PF^{c} ones. The PF^{ab} values are similar to those of the single-layer sample, pointing to an extrinsic reason for PF anisotropy.

Since ρ^{c} is larger than ρ^{ab} and S^{c} lower than S^{ab} in the thick sample, the power factor PF^{c} is thus much lower than PF^{ab}. At 900 K, PF^{c} and PF^{ab} values are in 42–46 and 495–555 μW m^{-1} K^{-2} ranges, respectively. The anisotropy ratio PF^{ab}/PF^{c} calculated from the average values reaches 12 at 900 K, corresponding to an increase of 20% in comparison with the value reported by Tani et al.[8]

3.3.3. Thermal conductivity

Fig. 7a shows the thermal conductivity, κ, measured in the 300–1000 K range on parallelepiped-shaped specimens cut parallel, κ^{ab}, and perpendicular, κ^{c}, to the mean c*-axis of the 30-layers stack. The thermal conductivity of the reference sample, κ^{ref}, was also plotted. Generally, κ decreases as the temperature is raised, in accordance with the curves reported for the bulk materials.[28–30]

κ can be expressed as the sum of a lattice component, κ_L, and an electronic component, κ_e ($\kappa = \kappa_L + \kappa_e$), which can be estimated following the Wiedemann–Franz law as:

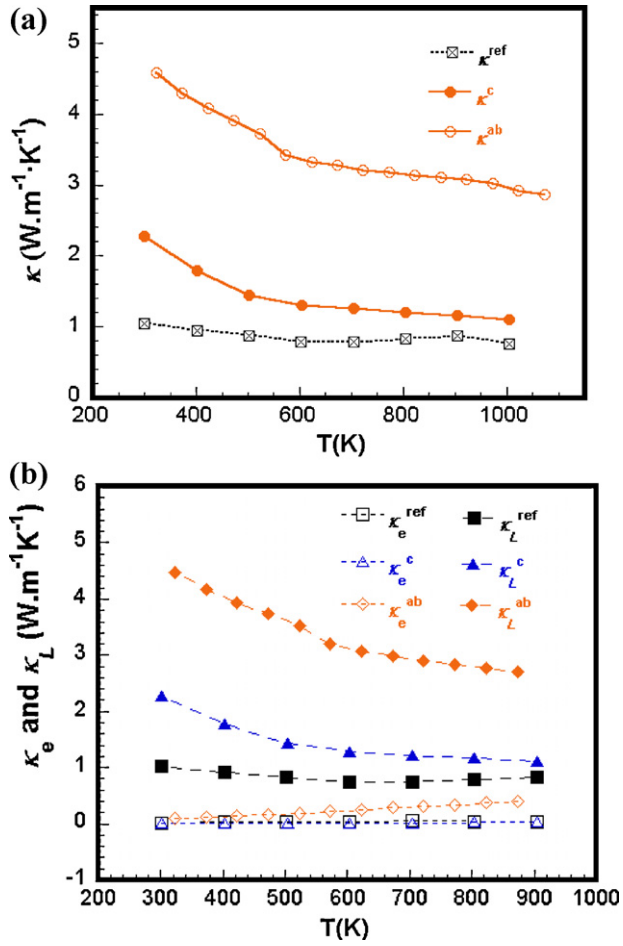

Fig. 7. (a) Temperature dependence of the thermal conductivity measured in the 300–1000 K range for the reference sample, κ^{ref}, and parallel, κ^{ab}, and perpendicular, κ^{c}, to the mean c-axis of the 30-layers stack. (b) Temperature dependence of the lattice component κ_L and the electronic component κ_e for κ^{ref}, κ^{ab} and κ^{c}.

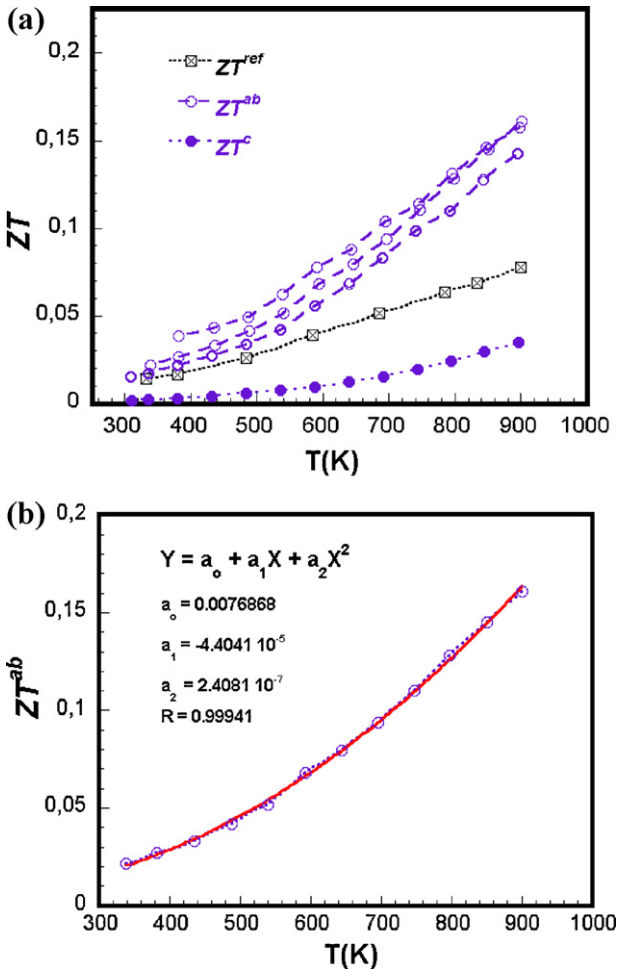

Fig. 8. (a) Temperature dependence of the resulting dimensionless figure-of-merit (ZT), in the 300-900 K range, for the reference sample, ZT^{ref}, and the 30-layers one in the directions parallel, ZT^{ab}, and perpendicular, ZT^{c}, to the mean c-axis. (b) Fit of the mean $ZT^{ab}(T)$ curves.

$\kappa_e = L{\cdot}\sigma{\cdot}T = L{\cdot}T/\rho$, where $L = 2.45 \times 10^{-8}\ V^2\ K^{-2}$ is the Lorentz number.[31] Since (κ^{ab}, ρ^{ab}), (κ^{c}, ρ^{c}) and (κ^{ref}, ρ^{ref}) decrease as T is raised, the contribution of κ_L is consequently more dominant than the contribution of κ_e to κ in $Ca_3Co_4O_9$ materials. Such results are clearly highlighted in Fig. 7b where $\kappa_L(T)$ and $\kappa_e(T)$ were plotted for κ^{ab}, κ^{c} and κ^{ref}.

On the other hand, κ_L is proportional to the mean free path of the phonons, l_L, as given by the kinetic formula: $\kappa_L = (1/3)C_D v_L l_L$, where C_D and v_L are the lattice specific heat and the phonon group velocity, respectively. A decrease in κ_L involves then a decrease in l_L supposing C_D and v_L unchanged. Such phenomena are reported to exist patently in the nanocrystal materials[32] due to phonon scattering at grain boundaries.

In fact, in the case of the reference sample, the large barriers (pores and/or grain boundaries) density influences phonon scattering, which reduces greatly l_L and, consequently, the lattice component, κ_L^{ref}. Otherwise, we reported in a previous work[7] larger ρ^{ref} values than ρ^{ab} measured for our single-layer and multilayer samples. Consequently, the electron component, κ_e^{ref} is also reduced, thanks to the Einstein relationship between κ_e and ρ. These results finally explain the lower κ^{ref} values.

Concerning the multilayer sample, its larger bulk density (95%) compared with the reference sample is one of the reasons explaining its larger κ. However, its κ^{ab} is much larger than κ^{c}, which is mainly related to the larger lattice component for κ^{ab} compared to κ^{c} (Fig. 7b). It comes from the lower mean free path l_L in the (a, b) planes, as a consequence of phonon scattering on a lower number of grain boundaries, compared to a conduction along the mean c*-axis. The electronic component for κ^{ab} is also larger than that for κ^{c}, due to the lower values of ρ^{ab} compared with ρ^{c}. It should be noticed that both the anisotropic character of the $Ca_3Co_4O_9$ structure and the texture[33] contributed also to increase κ^{ab} compared with κ^{c}. At 900 K, the multilayer sample exhibits $\kappa^{ab} = 3.1\ W\ m^{-1}\ K^{-1}$ and $\kappa^{c} = 1.15\ W\ m^{-1}\ K^{-1}$, which are 3.6 and 1.3 times, respectively, larger in comparison with the reference sample. The anisotropy ratio κ^{ab}/κ^{c} is then of 2.7. The κ^{ab} value is larger than those published for textured bulk materials by Wang et al.[28] ($1.96\ W\ m^{-1}\ K^{-1}$) and Zhang and Zhang[29] ($1.6\ W\ m^{-1}\ K^{-1}$). It is important to notice that most authors did not specify the direction of the thermal conductivity measurements on their materials, and Xu et al.[30] reported a κ value ($2.9\ W\ m^{-1}\ K^{-1}$) coherent to our obtained κ^{ab} at 900 K.

3.4. Figure-of-merit

Fig. 8a exhibits the temperature dependence of ZT, obtained in the 300–900 K range for the reference, ZT^{ref}, and in the directions parallel, ZT^{ab}, and perpendicular, ZT^{c}, to the mean c*-axis of the 30-layers sample. ZT^{ref}, ZT^{ab} and ZT^{c} increase monotonously as the temperature is raised in the whole investigated range, which testifies the performances stability of the $Ca_3Co_4O_9$ materials. ZT^{ab} values are the largest and the reference value coherently fits in the average, pointing then out the dominance of the resistivity reduction for the ZT improvement.

At 900 K, the mean ZT^{ab} value reached 0.16 and $ZT^{ab} = 2.1 \times ZT^{ref}$; the anisotropy ratio $ZT^{ab}/ZT^{c} = 4.6$, illustrating that the TE conversion efficiency of the textured $Ca_3Co_4O_9$ materials is much larger in their (a, b) planes than in those containing the c*-axis and also compared to the materials prepared by using the conventional sintering.

A good fit of the mean $ZT^{ab}(T)$ curve using a second order polynomial equation $ZT^{ab} = 0.0076868 - 4.4041 \times 10^{-5} \times T + 2.4081 \times 10^{-7} \times T^2$ is obtained (Fig. 8b). At 1000 K, the expected mean ZT^{ab} value is about 0.2.

4. Conclusions

We have demonstrated that the weak thickness of dense and strongly textured $Ca_3Co_4O_9$ (349) ceramics is no longer a limiting factor for their integration in practical thermoelectric (TE) modules. Henceforward, textured TE elements 'legs', with sufficient dimensions, can be cut from multilayer 349 TE materials fabricated by hot-pressing stacked thin single-layer samples, without using any soldering agent. Microstructure and volume quantitative texture studies showed a good quality of the interfaces between the layers and texture strength about 2 times larger than that of the single-layer sample. All TE properties, including the Seebeck coefficient, reveal an anisotropic character and can be compared to the ones of a single-layer along the (a, b) planes, while the resistivity ρ^{c} is considerably reduced compared with the single-layer sample.

The anisotropy ratios, ρ^{c}/ρ^{ab} and κ^{ab}/κ^{c}, of the resistivity and the thermal conductivity reached 13.5 and 2.7, respectively. The anisotropy ratio of the figure-of-merit is then $ZT^{ab}/ZT^{c} = 4.6$ at 900 K, indicative of the better TE conversion efficiency in the (a, b) planes of the textured $Ca_3Co_4O_9$ materials. At this temperature, the ZT^{ab} value is 0.16, which represents an improvement of 2 times in comparison with conventionally sintered 349 materials.

Acknowledgments

D. Kenfaui and the co-authors acknowledge the "Conseil Régional de Basse Normandie, France, Feder" for its PhD fellowship financial and financial participation to the experimental set-up used in this work.

References

1. Terasaki I, Sasago Y, Uchinokura K. Large thermoelectric power in $NaCo_2O_4$ single crystals. *Phys Rev B* 1997;**56**:R12685–7.
2. Masset AC, Michel C, Maignan A, Hervieu M, Toulemonde O, Studer F, et al. Misfit-layered cobaltite with an anisotropic giant magnetoresistance: $Ca_3Co_4O_9$. *Phys Rev B* 2000;**62**:166–75.
3. Fujita K, Mochida T, Nakamura K. High-temperature thermoelectric properties of $Na_xCoO_{2-\delta}$ Single Crystals. *Jpn J Appl Phys* 2001;**40**:4644–7.
4. Fergus JW. Oxide materials for high thermoelectric energy conversion. *J Eur Ceram Soc* 2012;**32**:525–40.
5. Bhattacharya S, Aswal DK, Singh A, Thinaharan C, Kulkarni N, Gupta SK, et al. Anisotropic electrical transport studies of $Ca_3Co_4O_9$ single crystals grown by the flux method. *J Cryst Growth* 2005;**277**:246–51.
6. Zhang Y, Zhang J, Lu Q. Synthesis of highly textured $Ca_3Co_4O_9$ ceramics by spark plasma sintering. *Ceram Int* 2007;**33**:1305–8.
7. Kenfaui D, Chateigner D, Gomina M, Noudem JG. Anisotropy of the mechanical and thermoelectric properties of hot-pressed single-layer and multi-layer thick $Ca_3Co_4O_9$ ceramics. *Int J Appl Ceram Technol* 2011;**1**(8):214–26.
8. Tani T, Itahara H, Xia C, Sugiyama J. Topotactic synthesis of highly-textured thermoelectric cobaltites. *J Mater Chem* 2003;**13**:1865–7.
9. Grimmer H. General relations for transport properties in magnetically ordered crystals. *Acta Cryst* 1993;**A49**:763–71.
10. Kenfaui D, Bonnefont G, Chateigner D, Fantozzi G, Gomina M, Noudem JG. $Ca_3Co_4O_9$ ceramics consolidated by SPS process: optimization of mechanical and thermoelectric properties. *Mat Res Bull* 2010;**45**:1240–9.
11. Sudhakar Reddy E, Noudem JG, Hébert S, Goupil C. Fabrication and properties of four-leg oxide thermoelectric modules. *J Phys D* 2005;**38**:3751–5.
12. Noudem JG, Lemonnier S, Prevel M, Reddy ES, Guilmeau E, Goupil C. Thermoelectric ceramics for generators. *J Eur Ceram Soc* 2008;**28**:41–8.
13. Funahashi R, Urata S. Fabrication and application of an oxide thermoelectric system. *Int J Appl Ceram Technol* 2007;**4**:297–307.
14. Rouessac V, Wang J, Provost J, Desgardin G. Processing and superconducting properties of highly textured Bi(Pb)-2223 ceramics by sinter-forging. *Physica C* 1996;**268**:225–32.
15. Chateigner D. *Combined analysis*. London: ISTE-Wiley; 2010, 496 p.
16. Rietveld HM. A profile refinement method for nuclear and magnetic structures. *J Appl Cryst* 1969;**2**:65–71.
17. Lutterotti L, Chateigner D, Ferrari S, Ricote J. Texture, residual stress and structural analysis of thin films using a combined X-ray analysis. *Thin Solid Films* 2004;**450**:34–41.
18. Lutterotti L, Matthies S, Wenk H-R. MAUD (material analysis using diffraction): a user friendly java program for rietveld texture analysis and more. In: Spunar JA, editor. *Textures of materials: proceedings of ICOTOM14*. Ottawa: National Research Council of Canada; 1999. p. 1599–604.
19. Montgomery HC. Method for measuring electrical resistivity of anisotropic materials. *J Appl Phys* 1971;**42**:2971–5.
20. Chateigner D. Reliability criteria in Quantitative texture analysis with experimental and simulated orientation distributions. *J Appl Crystallogr* 2005;**38**:603–11.
21. Prevel M, Lemonnier S, Klein Y, Hébert S, Chateigner D, Ouladdiaf B, et al. Textured $Ca_3Co_4O_9$ thermoelectric oxides by thermoforging process. *J Appl Phys* 2005;**98**:93706–9.
22. Nye JF. *Physical properties of crystals: their representation by tensors and matrices*. Lavoisier; 1985.
23. Yu L, Wang Y, Zhang PX, Habermeier H-U. Epitaxial $La_{0.9}Ca_{0.1}MnO_3$ films grown on vicinal cut substrates for the investigation of resistivity and thermoelectric anisotropy. *J Cryst Growth* 2011;**322**:41–4.
24. Sakai A, Kanno T, Yotsuhashi S, Okada S, H.Adachi. Preparation of meta stable $Sr_3Co_4O_9$ epitaxial thin films with controlled orientation and their anisotropic thermoelectric properties. *J Appl Phys* 2006;**99**:093704–7.
25. Kanno T, Yotsuhashi S, Adachi H. Anisotropic thermoelectric properties in layered cobaltite A_xCoO_2 (A = Sr and Ca) thin films. *Appl Phys Lett* 2004;**85**:739–42.

26. Th. Zahner, Stierstorfer R, Reindl S, Schauer T, Penzkofer A, Lengfellner H. Pico-second thermoelectric response of thin $YBa_2Cu_3O_{7-x}$ films. *Physica C* 1999;**313**:37–40 (no. 1–2).
27. Lengfellner H, Kremb G, Schnellbogl A, Betz J, Renk KF, W.Prettl. Giant voltages upon surface heating in normal $YBa_2Cu_3O_{7-\delta}$ films suggesting an atomic layer thermopile. *Appl Phys Lett* 1992;**60**:501–3.
28. Wang D, Chen L, Wang Q, Li J. Fabrication and thermoelectric properties of $Ca_{3-x}Dy_xCo_4O_{9+\delta}$ system. *J Alloy Compd* 2004;**376**:58–61.
29. Zhang Y, Zhang J. Rapid reactive synthesis and sintering of textured $Ca_3Co_4O_9$ ceramics by spark plasma sintering. *J Mater Proc Technol* 2008;**208**:70–4.
30. Xu G, Funahashi R, Shikano M, Pu Q, Liu B. High temperature transport properties of $Ca_{3-x}Na_xCo_4O_9$ system. *Solid State Commun* 2002;**124**:73–6.
31. Fine ME, Hsieh N. Wiedermann–Franz–Lorenz relation in highly electronic-conducting oxides. *J Am Ceram Soc* 1974;**57**:502–3.
32. Nolas GS, Sharp J, Goldsmid HJ. *Thermoelectrics, basic principles and new materials developments*. New York, NY: Springer; 2001.
33. Mikami M, Guilmeau E, Funahashi R, Chong K, Chateigner D. Enhancement of electrical properties of the thermoelectric compound $Ca_3Co_4O_9$ through use of large-grained powder. *J Mater Res* 2005;**20**(9): 2491–7.